Stopping and time reversing a light pulse using dynamic loss tuning of coupled-resonator delay lines

Sunil Sandhu,* M. L. Povinelli, and Shanhui Fan

Department of Electrical Engineering, Ginzton Laboratory, Stanford University, Stanford, California 94305, USA
**Corresponding author: centaur@stanford.edu*

Received July 23, 2007; revised October 15, 2007; accepted October 18, 2007;
posted October 19, 2007 (Doc. ID 85496); published November 12, 2007

We introduce a light-stopping process that uses dynamic loss tuning in coupled-resonator delay lines. We demonstrate via numerical simulations that increasing the loss of selected resonators traps light in a zero group velocity mode concentrated in the low-loss portions of the delay line. The large dynamic range achievable for loss modulation should increase the light-stopping bandwidth relative to previous approaches based on refractive index tuning. © 2007 Optical Society of America

OCIS codes: 130.3120, 200.4740, 210.0210, 230.0230.

Systems that dynamically manipulate the group velocity of light are of great interest in classical and quantum information processing [1,2]. For this purpose, dynamically tuned delay lines based on cascaded optical resonators have been well studied. In these systems, it was shown theoretically that by compressing the system bandwidth to zero, a light pulse can be stopped [3–8].

Dynamically tuned delay lines generally rely on refractive index tuning to achieve the required pulse delay. However, the input pulse bandwidth is limited by the tuning range of the refractive index. The operating bandwidth typically scales as $\delta n/n$ [9]. For the available index modulation strength of $\delta n/n \approx 10^{-4} - 10^{-3}$ in transparent semiconductors [10], the achievable bandwidth is on the order of 20–200 GHz for $\lambda = 1.5$ μm light. In contrast, the strength of loss modulation in semiconductors can be much larger. In this Letter, we introduce a light-stopping scheme based on loss tuning of coupled-resonator delay lines. The process should increase the allowable input pulse bandwidth as compared to index modulation systems.

The basic requirements of a light-stopping process are that the system supports a *large-bandwidth* state to accommodate the input pulse bandwidth, which is then tuned to a *narrow-bandwidth* state to stop the pulse [3]. In the following discussion, we give a general description of our proposed light-stopping process using loss modulation in the system shown in Fig. 1. The low-loss resonator in the unit cell has a static loss rate of γ_0, while the lossy resonator has a dynamic loss rate of $\gamma(t)$. The coupling rate between neighboring resonators is κ. In the initial state, one sets $\gamma(t) = \gamma_0$; the system therefore consists of a chain of essentially lossless resonators ($\gamma_0 \ll \kappa$) with coupling rate κ large enough to accommodate the input pulse bandwidth. Once the pulse is within the system, the loss rate $\gamma(t)$ in every other resonator is tuned to $\gamma_{stop} \gg \kappa$. As a result, the system is brought to a narrow-bandwidth state. In this narrow-bandwidth state, the low-loss resonators are essentially decoupled from the lossy resonators, and the signal energy is trapped in the low-loss resonators. In this light stopping process, as long as one can get a large dynamic range of loss modulation, one can choose a large κ and, hence, accommodate a large pulse bandwidth in the initial state.

During the tuning process, the pulse energy loss peaks near $\gamma(t) = \kappa$, which defines a *critical-damping* point. To minimize the overall loss that the pulse experiences, the system should spend as little time as possible in the vicinity of the critical-damping point [i.e., the dynamic tuning of $\gamma(t)$ should be performed as rapidly as possible]. Hence, dynamic tuning of the system to the narrow-bandwidth state is performed nonadiabatically. This is in contrast to the adiabatic

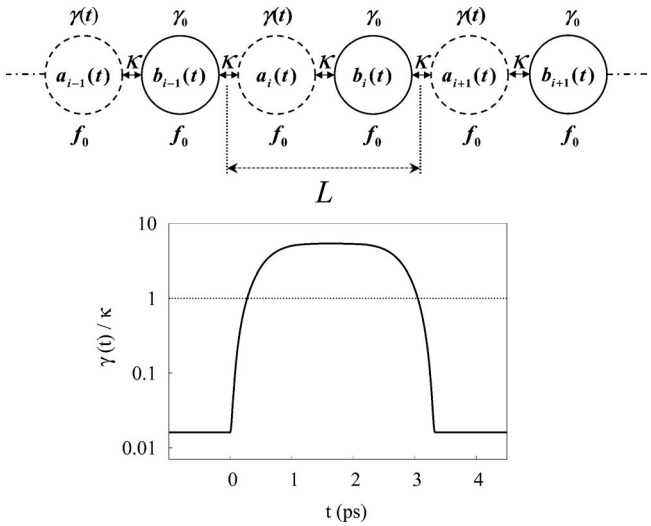

Fig. 1. Top diagram shows a section of the coupled-resonator light-stopping system. The unit cell has length L and consists of a lossy resonator with dynamic loss $\gamma(t)$ and a low-loss resonator with static loss γ_0. The bottom plot shows the modulation performed on $\gamma(t)$, with the dotted line indicating the critical-damping point.

0146-9592/07/223333-3/$15.00

tuning performed in light-stopping systems using index modulation [3].

We now perform a detailed numerical analysis of the light-stopping system in Fig. 1. The system can be described by the following coupled-mode equations, which have previously been shown to accurately describe light propagation in dynamic photonic-crystal resonator systems [3]:

$$\frac{1}{2\pi}\frac{d\mathbf{a}_i(t)}{dt} = (jf_0 - \gamma(t))\mathbf{a}_i(t) + j\kappa\mathbf{b}_i(t) + j\kappa\mathbf{b}_{i-1}(t), \quad (1)$$

$$\frac{1}{2\pi}\frac{d\mathbf{b}_i(t)}{dt} = (jf_0 - \gamma_0)\mathbf{b}_i(t) + j\kappa\mathbf{a}_{i+1}(t) + j\kappa\mathbf{a}_i(t). \quad (2)$$

The unit cell consists of two resonators with mode amplitudes $\mathbf{a}_i(t)$ and $\mathbf{b}_i(t)$. Each resonator has a static resonance frequency f_0. Tuning of $\gamma(t)$ is performed such that discrete translation symmetry of the system is always maintained. The complex eigenfrequencies of the system are given by

$$f = f_0 + j\frac{\gamma(t) + \gamma_0}{2} \pm \sqrt{2\kappa^2\cos^2\left[\frac{kL}{2}\right] - \left(\frac{\gamma(t) - \gamma_0}{2}\right)^2}, \quad (3)$$

where k is the Bloch wave vector. Equation (3) defines two bands that we refer to as the *lower band* ($-$ sign) and the *upper band* ($+$ sign).

Figure 2(a) shows the complex frequency f of the system in its initial state with loss $\gamma(t) = \gamma_0 \ll \kappa$. There is no splitting of Re[f] at $k = \pi/L$, and both bands have the same loss. Since the upper band has very high loss for $\gamma(t) \gg \kappa$ [Figs. 2(b) and 2(c)], we focus on the lower band in the following discussion. The quality factor $Q = f_0/2\,\mathrm{Im}[f]$ of the lower band has a peak value of $f_0/2\gamma_0$ at $k = \pi/L$. The peak is independent of $\gamma(t)$ because the $k = \pi/L$ state has all its energy in the low-loss resonator. At the critical-damping point $\gamma(t) = \kappa$ [Fig. 2(b)], the peak has a minimum width in k space and the overall loss is largest. As $\gamma(t)$ is tuned above κ, the width of the quality factor peak starts to increase, which translates to a decrease of loss for states near $k = \pi/L$. For $\gamma(t) \gg \kappa$, the entire lower band and upper band are associated with the low-loss and lossy resonators, respectively [Fig. 2(c)]. The frequency bandwidth of both bands becomes very narrow, and the group velocity of the signal is zero.

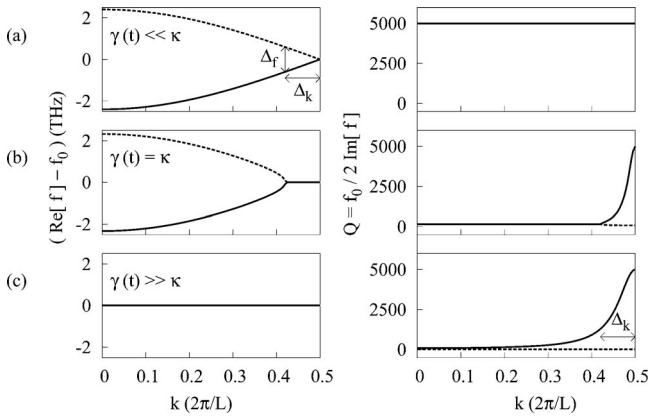

Fig. 2. Band structure for the system shown in Fig. 1. The left column shows (Re[f]$-f_0$), while the right column shows $Q = f_0/2\,\mathrm{Im}[f]$. Δ_f and Δ_k denote, respectively, the width in frequency and in wave vector space occupied by a Gaussian pulse with a bandwidth of 0.4 THz. (a) Initial state $\gamma(t) \ll \kappa$, where Q of both lower and upper bands are equal and constant for all k vectors. (b) Critical-damping point $\gamma(t) = \kappa$. (c) Narrow-bandwidth state $\gamma(t) \gg \kappa$, where Re[f] of both lower and upper bands are equal and constant for all k vectors.

To study pulse propagation during the dynamic process, the coupled equations [Eqs. (1) and (2)] were solved numerically for a system of $N = 70$ unit cells. A Gaussian input signal with bandwidth (full width at half-maximum of the intensity) of 0.4 THz and center frequency $f_c = 193$ THz was used [Fig. 3(a)]. The coupling constant $\kappa = 1.2$ THz and resonant frequency $f_0 = 193$ THz were chosen so that the pulse would occupy a frequency width Δ_f in the linear region of the system bandwidth, and a k-space region with width Δ_k near $k = \pi/L$, which is the low-loss region for large $\gamma(t)$ [Fig. 2(c)]. Since discrete translational invariance is maintained during the tuning of $\gamma(t)$, the pulse occupies the same k-space region close to $k = \pi/L$ during the entire process [Figs. 2(b) and 2(c)]. $\gamma(t)$ was dynamically tuned from $\gamma_0 = 193\ \mathrm{THz}/(2\times5000)$ to $\gamma_{\mathrm{stop}} = 193\ \mathrm{THz}/(2\times15)$ in 1 ps (Fig. 1), stopping the pulse [Fig. 3(b)]. After a holding time of 1.33 ps, the same dynamic process was applied in reverse to retrieve the signal. Figure 3(c) shows the pulse output, which consists of a forward pulse and a backward time-reversed pulse [11] of the same amplitude. Notice that the pulses are still Gaussian.

We now comment in detail on the loss mechanism during the dynamic process. During the stopping process [i.e., from Fig. 3(a) to Fig. 3(b)], approximately half the signal energy is lost because half the input pulse occupies the upper band, which acquires a high loss as $\gamma(t)$ is tuned to γ_{stop}. The remaining signal energy loss in this period occurs during the nonadiabatic $\gamma_0 \rightarrow \gamma_{\mathrm{stop}}$ tuning through the critical-damping point $\gamma(t) = \kappa$. During the storage period [Fig. 3(b)],

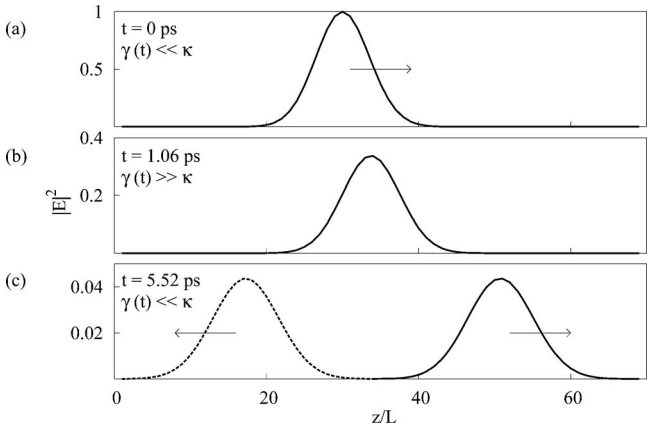

Fig. 3. Spatial signal profile from coupled-mode analysis: (a) input pulse, (b) pulse in narrow-bandwidth stop state, (c) output pulses.

loss arises due to attenuation of the signal in the narrow-bandwidth stop state. The attenuation of the signal during the narrow-bandwidth state as well as the slight increase in pulse width can be reduced by increasing the ratio γ_{stop}/κ, which increases the width in the k space associated with the lower band quality factor [Fig. 3(c)]. During the release process [i.e., from Fig. 3(b) to Fig. 3(c)], additional loss results from the nonadiabatic tuning of $\gamma(t)$, which leads to signal leakage into the upper band and a backward time-reversed pulse [Fig. 3(c)].

We note that in the coupled-mode theory, it is assumed that the loss of the lossy resonators can be increased without any effect on the low-loss resonators. We have performed finite-difference time domain (FDTD) [12] simulations of a 2D coupled resonator photonic crystal system similar to Fig. 1. We have verified that the shape of the $Q(k)$ curve in the narrow-bandwidth state [Fig. 2(c)] agrees with the coupled-mode theory. Thus, the coupled-mode theory accurately describes the dynamic light-stopping process. Due to field penetration effects, there is an additional signal loss not captured in the coupled-mode theory. However, we have verified that for the example shown here, this additional signal loss is minimal.

We observe in the simulation that the backward time-reversed pulse has the same amplitude as the forward pulse. This effect can be explained as follows: consider a particular wave vector point k_0 within the spatial spectrum of the signal. At the start of the pulse release process, the signal energy at k_0 is completely within the lower band. In addition, the value of Re[f] for both lower and upper bands is constant and equal [Fig. 2(c)]. As $\gamma(t)$ is decreased during the pulse release process, the values of Re[$f(k_0)$] for the lower and upper bands split when the losses Im[$f(k_0)$] become equal [Eq. (3)]. The band splitting is in equal and opposite directions. As a result, the signal energy from the initially flat lower band at k_0 is distributed equally among the lower and upper bands. Since discrete translational invariance is maintained throughout the tuning process, this argument can be generalized to all wave vector points within the spatial spectrum of the signal.

In the above numerical simulation, the modulation performed on $\gamma(t)$ corresponds to modulating the material loss from $\alpha=14$ cm^{-1} to $\alpha=4500$ cm^{-1} in a time of 1 ps ($\alpha \equiv \gamma/v$, where v is the group velocity in the bulk material). In InGaAs/InP quantum wells operating at room temperature, tuning the material loss from $\alpha=1500$ cm^{-1} to $\alpha \approx 0$ cm^{-1} has been demonstrated [13]. Moreover, the intrinsic response time of this system is in the femtosecond range [14]. It is likely that a higher contrast ratio of the material loss can be accomplished at a lower operating temperature. In silicon devices tuned via free carrier injection, achieving a material loss of $\alpha=4500$ cm^{-1} requires an injected carrier density of $\approx 4\times10^{20}$ cm^{-3}, which may be achievable in heavily doped structures [15]. In such a system one needs to remove most of the carriers to achieve the low material loss value of $\alpha=14$ cm^{-1}. This can potentially be achieved with a reverse bias structure [16]. The modulation time is fundamentally limited by the carrier lifetime. In silicon photonic crystals, the carrier lifetime can be reduced by manipulating the degree of surface passivation to obtain strong surface recombination or by using ion implantation [10]. For example, a carrier lifetime of less than 1 ps has been demonstrated in ion-implanted Si [17].

This work is supported in part by the United States Air Force Office of Scientific Research (AFOSR) grant FA9550-05-0414 and the Packard Foundation. The authors thank D. A. B. Miller and Onur Fidaner for discussions.

References

1. C. Liu, Z. Dutton, C. H. Behroozi, and L. V. Hau, Nature **409**, 490 (2001).
2. D. F. Phillips, A. Fleischhauer, A. Mair, R. L. Walsworth, and M. D. Lukin, Phys. Rev. Lett. **86**, 783 (2001).
3. M. F. Yanik and S. Fan, Phys. Rev. Lett. **92**, 083901 (2004).
4. Z. S. Yang, N. H. Kwong, R. Binder, and A. L. Smirl, Opt. Lett. **30**, 2790 (2005).
5. J. B. Khurgin, Phys. Rev. A **72**, 023810 (2005).
6. S. Sandhu, M. L. Povinelli, M. F. Yanik, and S. Fan, Opt. Lett. **31**, 1985 (2006).
7. S. Longhi, Phys. Rev. E **75**, 026606 (2007).
8. Q. Xu, P. Dong, and M. Lipson, Nat. Phys. **3**, 406 (2007).
9. M. F. Yanik and S. Fan, Phys. Rev. A **71**, 013803 (2005).
10. M. Lipson, J. Lightwave Technol. **23**, 4222 (2005).
11. M. F. Yanik and S. Fan, Phys. Rev. Lett. **93**, 173903 (2004).
12. A. Taflove and S. C. Hagness, *Computational Electrodynamics* (Artech House, 2000).
13. I. Bar-Joseph, C. Klingshirn, D. A. B. Miller, D. S. Chemla, U. Koren, and B. I. Miller, Appl. Phys. Lett. **50**, 1010 (1987).
14. W. H. Knox, D. S. Chemela, D. A. B. Miller, J. B. Stark, and S. Schmitt-Rink, Phys. Rev. Lett. **62**, 1190 (1989).
15. R. A. Soref and B. R. Bennett, IEEE J. Quantum Electron. **23**, 123 (1987).
16. H. Rong, R. Jones, A. Liu, O. Cohen, D. Hak, A. Fang, and M. Paniccia, Nature **433**, 725 (2005).
17. A. Chin, K. Y. Lee, B. C. Lin, and S. Horng, Appl. Phys. Lett. **69**, 653 (1996).